PROCEEDINGS OF SCIENCE

Gamma-ray burst detection with particle detectors of LEO satellites

Coralie Neubüser[a,*] **on behalf of the Limadou/HEPD-01 Collaboration**

[a] *TIFPA-INFN,*
Via Sommarive 14, 38123 Trento, Italy

E-mail: coralie.neubueser@tifpa.infn.it

Intense and long gamma-ray bursts (GRBs) can be seen from Earth when happening in close-by universes. As seen in the case of the recent, giant, long-lasting GRB221009A. GRB221009A originated from a collapsing star and was found at a redshift of 0.152. The event was observed by many gamma-ray detectors onboard different satellites as well as underground Very Low Frequency (VLF) antennas. An exceptionally large flux of high energy photons was measured with a peak emission of >1.8 millions/cm^2/s. The illumination of the Earth was centered on India and included Europe and Asia. We report on the observation of sudden electron flux changes, measured by multiple charge particle instruments, including the HEPP-L detector on-board the China Seismo-Electromagnetic Satellite (CSES), and discuss the position and orientation dependence. The time structure of the electron flux changes of the GRB221009 closely matches the very distinctive time dependence of the photon flux associated with the main double peaked emission observed at around 13:20 UTC. The observed signal was found to originate mostly from Compton scattered electrons at the aluminium collimators, providing a real time monitoring of very intense photon fluxes.

38th International Cosmic Ray Conference (ICRC2023)
26 July - 3 August, 2023
Nagoya, Japan

*Speaker

PoS(ICRC2023)689

1. Introduction

Gamma-ray bursts (GRBs) are generated by highly energetic astrophysical events, producing intense photon bursts reaching Earth after a long journey in space. For their neutral nature and low cross section to intergalactic matter, they travel without being perturbed by magnetic fields, thus the Universe is highly transparent to their passage up to very high redshift. The measurement of the characteristics of these events (time structure and energy spectrum) has been key to understand the nature of their progenitors and to model the relativistic emission processes generating the most energetic phenomena. Thus, these data play an important role in observational astrophysics, by providing an unique tool for the study of the evolution and its chemical composition. Long-lasting GRBs are rare events, and the brightest, in terms of flux measurable on Earth, occur only every few years. Their maximum flux is usually in the MeV range, and at higher energies the probability of detecting a GRB photon decreases exponentially.

On October 9th 2022, at 13:16:59 UTC, telescopes on board Earth-orbiting satellites detected the brightest long gamma-ray burst ever recorded in the history of observational astrophysics [1]. GRB221009A was located at RA= +19h 14m 03s and Decl=+19d 50' 33", which corresponds to a zenith over India, at about +71° longitude and +19.8° latitude. The GRB illuminated most of Europe, Asia, Africa and Australia. The highest photon energy reported in association with this GRB has been measured at 18 TeV by the LHAASO [2] ground array experiment in China. The GRB triggered several space-based instruments sensitive to gamma rays, such as Swift with the Burst Alert Telescope (BAT) [3], FERMI with the Gamma-ray Burst Monitor (GBM) [4] and INTEGRAL [5] with its Burst Alert System (IBAS) [6]. Measurements have also been performed by the Spectrometer/Telescope for Imaging X-rays (STIX) on Solar Orbiter [7], PICsIT and SPI/ACS on INTEGRAL [5] and HEBS on SATech-01 [8]. The main component of the GRB221009A was so intense, that most gamma-ray burst monitors showed signs of saturation during the main GRB emission, between 13:20:40 and 13:21:30 UTC. HEBS, however, followed the main part of gamma flux evolution without data saturation and sub-second timing resolution: for this reason HEBS data [9] was used as reference in this work.

The extraordinary brightness of GRB221009A triggered the suspicion that secondary electrons might have been created either in the interaction with the ionosphere or the direct interaction with the detector material of instruments onboard Low Earth Orbit (LEO) satellites. Thus the electron flux of HEPP-L, the low-energy particle detector on board the China Seismo-Electromagnetic Satellite (CSES-01) [10], was investigated and a simultaneous increase in the electron flux was observed [11]. This, together with a Geant4 simulation confirmed the creation of electrons through the photon absorption in the detector material. In addition, the low energy electron fluxes measured by the Medium Energy Proton and Electron Detector (MEPED) onboard various other satellites (NOAA POES and METOP) were utilized to study the response to the GRB221009A [**?**]. And also in these cases, an instantaneous flux enhancement could be observed when the satellite was located in the illuminated area and the background electron flux was not too high (e.g. outside the South Atlantic Anomaly).

In the following, we will discuss in detail the signal significances, the sensitivity of the instruments depending on their orbital location and summarize with an outlook.

2. Low energy electron detectors onboard LEO satellites

2.1 MEPED onboard NOAA POES

The MEPED detector consist of two proton and two electron telescopes, each. These are oriented at 0 and at 90° from Zenith, respectively. A schematic of the proton telescope is shown in Figure 1b. The electron telescope is similar but has a single Silicon sensor of 700 μm thickness, which can fully contain incident electrons with energies up to ~2.5 MeV, and no magnet. Instead, a nickel foil is used to block incident protons which reduces the proton contamination down to 20 % [12]. The electron fluxes are finally calculated above four energy thresholds: 0.04, 0.13, 0.287, and 0.612 MeV. The electron flux above 612 keV is based on the measurement of the proton telescope. The geometrical factors used for the flux estimations from particle rates are given in Table 1, together with the active area of the Silicon sensor.

	geometrical factor [cm^2·s·sr]	active area [mm^2]
MEPED	(1.24/1.44/0.75/0.55)/100	25
HEPP-L	0.12/0.73	300

Table 1: Geometrical factor and active area of the MEPED electron telescopes for the 4 energy thresholds and the HEPP-L detector for the narrow and wide collimators.

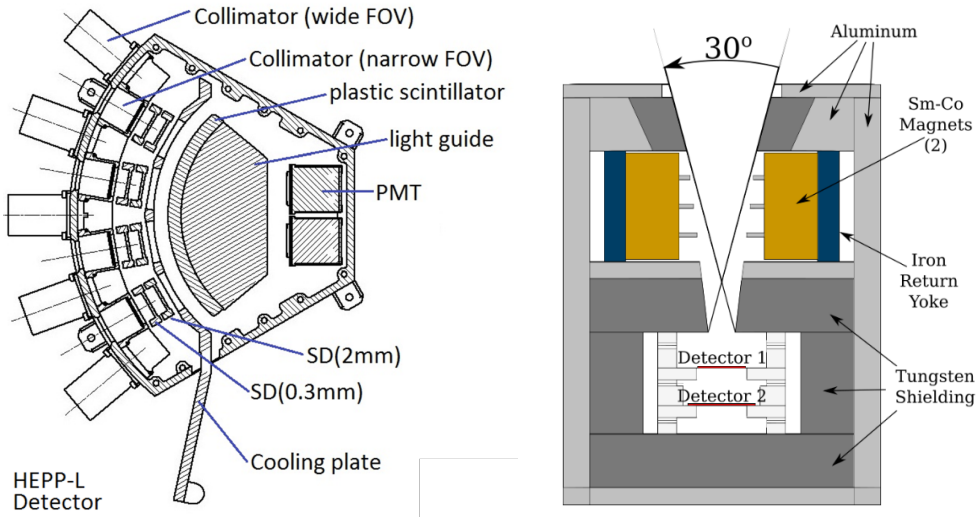

(a) **(b)**

Figure 1: (a) The schematic of the HEPP-L detector with the 4 and 5, wide and narrow collimators with two silicon detectors, each [13]. (b) A schematic view of the MEPED proton telescope [12], which consists of two silicon detectors (each 200 μm thick) and a collimator with angular half-width of 15° and a similar inner collimator has half-width of 6.5°. A magnet of 0.25 T is used to deflect electrons.

2.2 HEPP-L onboard CSES-01

The HEPP-L detector consists of 4 and 5 Silicon units with wide and narrow collimators of 13 and 30° opening angle, respectively. The top view of the instrument is given in Figure 1a. Each Silicon unit is made of two Silicon sensors with 300 μm and 2 mm thickness that are stacked on top of each other. Both measure the deposited energy of the passing particles, which enables particle identification via a dE/dx measurement and results in an electron idenfication efficiency of 96.7 % [13]. An additional anti-coincidence detector made of a plastic scintillator with Photo-Multiplier Tube (PMT) readout, ensures containment. This instrument covers an electron energy range from 100 keV up to 3 MeV, with an energy resolution of 11 keV.

3. Results

Figure 2 shows the electron flux measured on October 9th 2022 from 13:20 to 13:26 UTC by (a) the HEPP-L of CSES-01 and (b) the electron telescope onboard NOAA POES-19 oriented at 0°. Both flux profiles are confronted with the photon counts measured by HEBS and exhibit two simultaneous peaks. The electron flux measured by all HEPP-L channels reproduces well the inner structures of the photon peaks and shows even a slight enhancement in conjunction with the third much smaller peak around 13:25:29 UTC. For this comparison the lowest energies were excluded to minimise the electron background of the inner radiation belt, which is crossed in that moment. The electron flux of the 0° and 90° telescopes onboard NOAA POES-19 see a simultaneous flux increase with the photon counts, but the agreement in the peak timing is not as good as shown for HEPP-L. Overall, there is a shift towards a later occurrence, which lies within the 2 s time resolution.

Additionally, we have studied the significance of the GRB signals against the electron flux background which is estimated in the invariant phase-space of L-shell and equatorial pitch angle (L-α_{eq}) on a daily basis. After the background estimation, the fluxes above a threshold (variable in the number of σ, here 3), which are called seeds are clustered and build a particle burst (PB) if two consecutive seeds were found. Afterwards, a time window is opened (here 5s) and all other seeds within that window are added to the PB. A more detailed description of the definitions and procedures is described in [14]. Figure 3 shows the flux profiles within 3 minutes of the GRB for channel 0 of HEPP-L (left) and the 0° telescope of NOAA POES-19 (right). The figures on the top contain the fluxes for 2 energy bins or thresholds, together with the estimated threshold for signals above 3σ. The bottom figures present the final output of the clustering algorithm in terms of PBs. Each shaded block represents a PB, with the curves showing the single fluxes that make up the burst. The y-axis shows the significance of the fluxes.

The HEPP-L signals are shown for two out of 11 energy bins, which had been applied offline to simplify the analysis and to ensure a stable background estimation. The found PBs exhibit a significance of 120 to 130 σ for the first and 20 to 50 σ for the second peak. The signals seen in the 0° electron telescope of NOAA POES-19 reach significances of 60 to 75 σ for the first and 15 to 25 σ for the second peak. It must however be mentioned that these are fluxes measures above two energy thresholds, which renders these results highly correlated.

As shown in [11], the observation of the GRB signal across many energy bins in HEPP-L results in a probability of such an event to occur due to a statistical fluctuation to be lower than 10^{-7}.

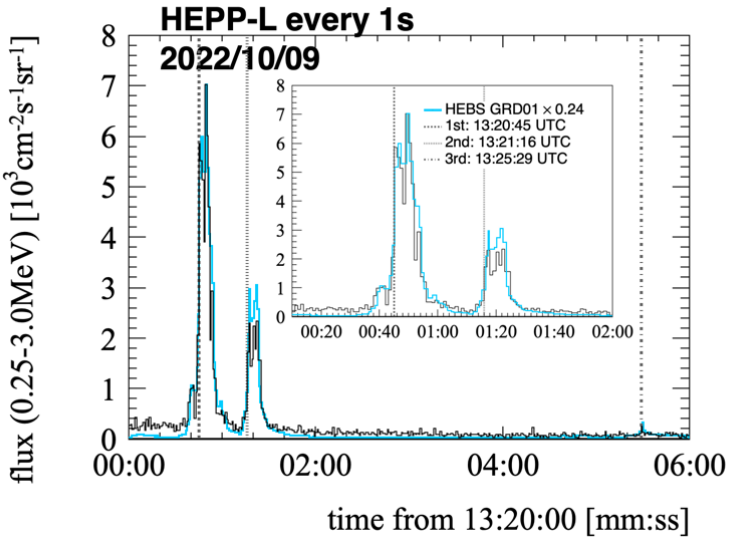

(a)

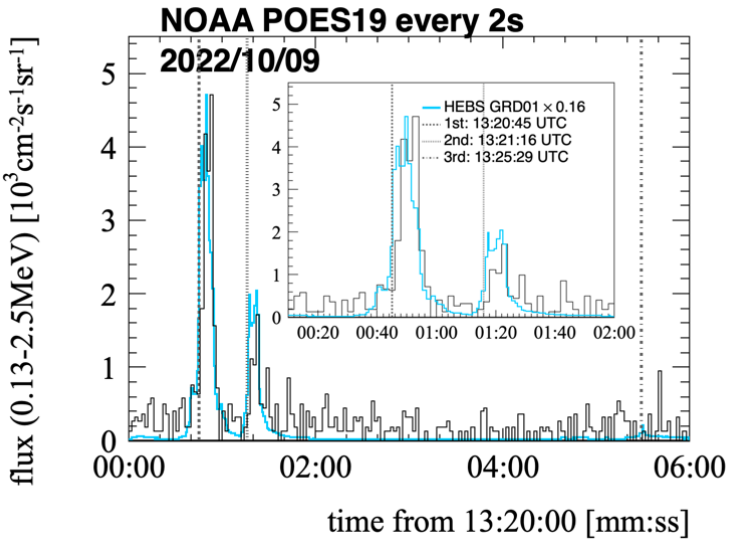

(b)

Figure 2: Electron flux of; (a) all HEPP-L channels summed over the energy range from 250 keV to 3 MeV [11], (b) the NOAA POES-19 both electron telescopes summed over the energy range from 130 keV to 2.5 MeV on 09.10.2022 starting from 13:20:00 UTC. The blue curve shows the measured photon counts per second of the HEBS GRD01 instrument [9], scaled to match the maximum of the first peak. The scaling factors are given in the legend.

To study an eventual orientation dependence of the instruments with respect to the GRB origin, we have further extended the analysis to the detectors oriented at about 90° from Zenith. The signal fluxes and significances for the channel 5 (~92°) of HEPP-L and the 90° electron telescope of NOAA POES-19 are shown in Figure 4. In case of the HEPP-L results (left), the low-energy

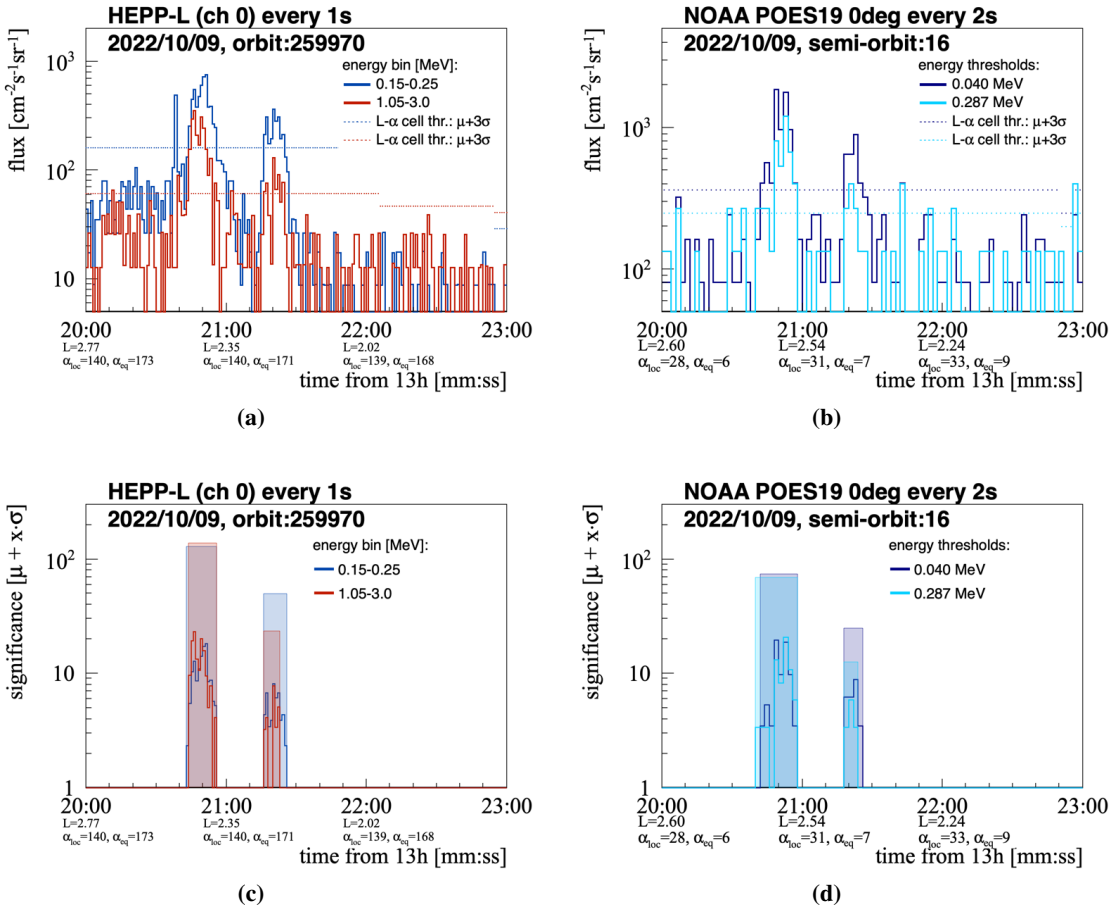

Figure 3: (a) The flux profile versus time for channel 0 of HEPP-L. The blue and red curves show the flux corresponding to the second lowest (150-250 keV) and highest (1.05-3 MeV) energy bin, respectively. (b) The flux profile versus time for the electron telescope of NOAA POES-19 satellite in 0°. The dark and light blue curves correspond to the flux measured above the lowest (40 keV) and second highest (287 keV) energy threshold, respectively. The horizontal lines mark the threshold of 3σ above the average for the corresponding L-α_{eq} bins. (c,d) The significance of the single flux (histogram) and the particle bursts (shaded area) given in the number of standard deviations above the background.

electron background of the inner radiation belt is very well visible for the (150-250) keV energy bin. For energies above 250 keV this background vanishes and the PB algorithm identifies the GRB signal with a high significance of about 140 and 28 σ for the the first and second peak, respectively. The signals seen by the 90° telescope of the NOAA POES-19 satellite show the same background of low-energy electrons emerging at these L-shells larger than 2, which prevents the detection of the GRB in the very low energy regime. But for the highest two energy thresholds (here shown 612 keV) the first peak is still detectable above the background with a significance of 40 σ.

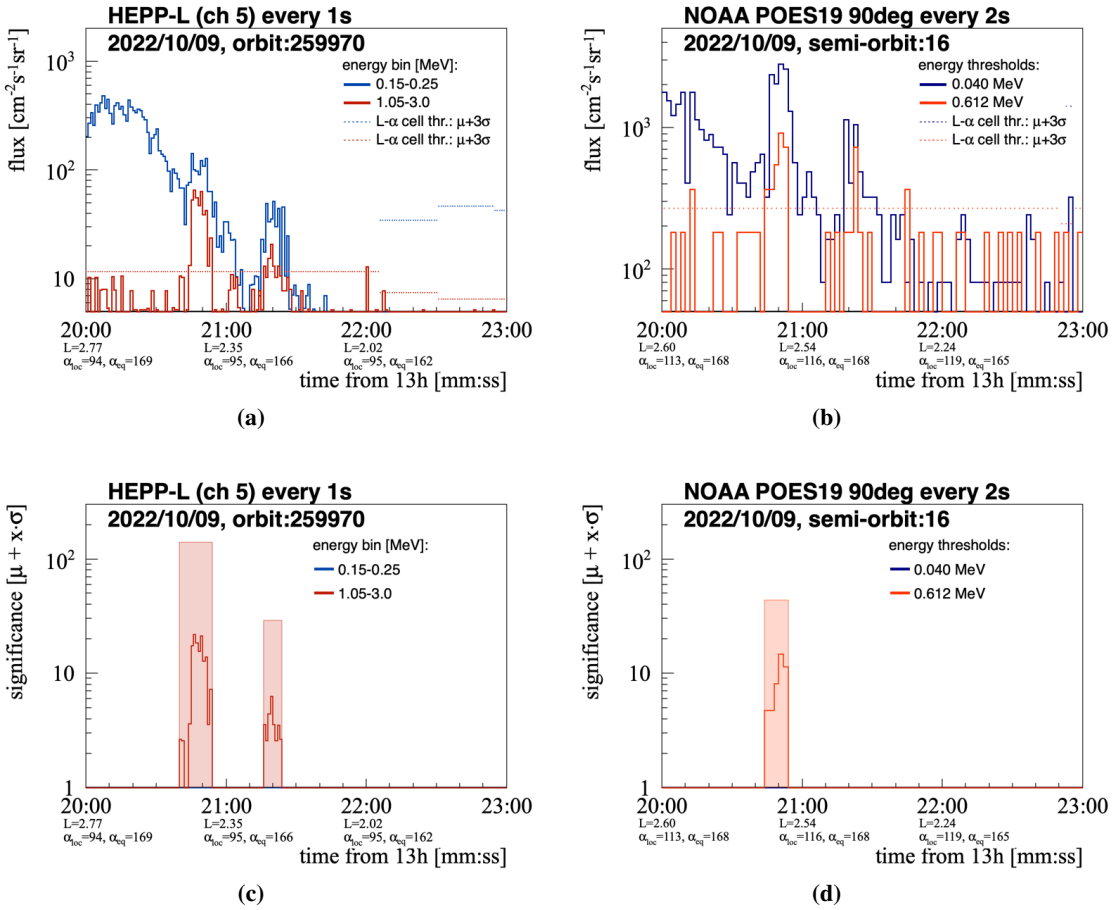

Figure 4: (a) The flux profile versus time for channel 5 of HEPP-L. The blue and red curves show the flux corresponding to the second lowest (150-250 keV) and highest (1.05-3 MeV) energy bin, respectively. (b) The flux profile versus time for the electron telescope of NOAA POES-19 satellite in 90°. The blue and red curves correspond to the flux measured above the lowest (40 keV) and second highest (612 keV) energy threshold, respectively. The horizontal lines mark the threshold of 3σ above the average for the corresponding L-α_{eq} bins. (c,d) The flux significance of the single flux (histogram) and the particle bursts (shaded area) given in the number of standard deviations above the background.

4. Conclusions

We have investigated the possibility to detect the GRB221009A with electron detectors onboard LEO satellites and found enhanced electron fluxes that match the time structure of the observations by specialised GRB photon observatories. From these observations and basic Geant4 simulations, we conclude that the signal observed in HEPP-L is due to prompt production of low-energy electrons in the passive material surrounding the sensitive Silicon detectors, providing a full solid angle coverage without any need of pointing accuracy. We have demonstrated that the GRB221009A signal significance lays around 20-130 σ above the average electron fluxes, in the case of low background fluxes (outside the radiation belts, i.e. outside the detectors sensitivity to trapped electron fluxes within the radiation belts). We have expanded this analysis to other GRBs, that had

about a factor 50 lower intensity, but could up to now not find another case of GRB detection.

References

[1] E. Burns et al., "GRB 221009A: The BOAT," *The Astrophysical Journal Letters*, vol. 946, p. L31, mar 2023.

[2] Y. Huang, S. Hu, S. Chen, et al., "Lhaaso observed grb 221009a with more than 5000 vhe photons up to around 18 tev," tech. rep., GCN Circ. 32677, 2022.

[3] S. Dichiara et al., "Swift J1913.1+1946 a new bright hard X-ray and optical transient," tech. rep., GCN Circ. 32632, 2022.

[4] S. Lesage, P. Veres, O.J. Roberts, E. Burns, E. Bissaldi et al., "Grb 221009a: Fermi gbm observation," tech. rep., GCN Circ. 32642, 2022.

[5] D. Götz, S. Mereghetti, V. Savchenko, C. Ferrigno, E. Bozzo et. al., "Grb221009a/swift j1913.1+1946: Integral spi/acs observations," tech. rep., GCN Circ. 32660, 2022.

[6] S. Mereghetti, D. Götz, J. Borkowski, R. Walter, H. Pedersen, "The integral burst alert system," *A&A*, vol. 411, no. 1, pp. 291–297, 2003.

[7] H. Xiao, S. Krucker, R. Daniel et. al., "Grb221009a/swift j1913.1+1946: Solar orbiter stix measurements.," tech. rep., GCN Circ. 32661, 2022.

[8] J. C. Liu, Y. Q. Zhang, S. L. Xiong et al., "Grb 221009a: Hebs detection," tech. rep., GCN Circ. 32751, 2022.

[9] J. C. Liu, Y. Q. Zhang, S. L. Xiong et al., "http://twiki.ihep.ac.cn/pub/GECAM/GRBList/HEBS-GRB221009A.png." 2022.

[10] X. Shen et al., "Introduction to special section on the china seismo-electromagnetic satellite and initial results," *Earth and Planetary Physics*, vol. 2, no. 1, p. 439, 2018.

[11] R. Battiston et al., "Observation of Anomalous Electron Fluxes Induced by GRB221009A on CSES-01 Low-energy Charged Particle Detector," *The Astrophysical Journal Letters*, vol. 946, p. L29, mar 2023.

[12] K. Yando et al., "A Monte Carlo simulation of the NOAA POES Medium Energy Proton and Electron Detector instrument," *JGR: Space Physics*, vol. 116, no. A10, 2011.

[13] X.Q. Li et al., "The high-energy particle package onboard CSES," *Radiat. Detect. Technol. Methods*, vol. 3, p. 22, 2019.

[14] C. Neubüser et al., "Search for Electron Bursts in the Inner Van Allen Belts with the CSES and NOAA POES Satellites," *Remote Sens.*, vol. 15, no. 411, 2023.

Full Authors List: Limadou/HEPD-01 Collaboration

S. Bartocci[a], R. Battiston[b,c], W. J. Burger[c], D. Campana[d], G. Castellini[e], P. Cipollone[a], L. Conti[f,a], A. Contin[g,h], C. De Donato[a], C. De Santis[a], F. M. Follega[b,c], G. Gebbia[b,c], R. Iuppa[b,c], M. Lolli[h], M. Martucci[a], G. Masciantonio[a], M. Mergè[i,a], M. Mese[l,d], C. Neubüser[c], F. Nozzoli[c], A. Oliva[h], G. Osteria[d], L. Pacini[m], F. Palma[a], F. Palmonari[g,h], B. Panico[l,d], F. Perfetto[d], P. Picozza[n,a], M. Pozzato[h], E. Ricci[b,c], M. Ricci[o], S. B. Ricciarini[e], Z. Sahnoun[g,h], V. Scotti[l,d], A. Sotgiu[a], R. Sparvoli[n,a], V. Vitale[a], S. Zoffoli[i] and P. Zuccon[b,c]

[a] INFN-Sezione di Roma "Tor Vergata", Via della Ricerca Scientifica 1, I-00133 Roma, Italy
[b] University of Trento, Via Sommarive 14, I-38123 Povo (Trento), Italy
[c] INFN-TIFPA, Via Sommarive 14, I-38123 Povo (Trento), Italy
[d] INFN-Sezione di Napoli, Via Cintia, I-80126 Napoli, Italy
[e] IFAC-CNR, Via Madonna del Piano 10, I-50019 Sesto Fiorentino (Firenze), Italy
[f] Uninettuno University, Corso V. Emanuele II 39, I-00186 Roma, Italy
[g] University of Bologna, Viale Berti Pichat 6/2, Bologna, Italy
[h] INFN-Sezione di Bologna, Viale Berti Pichat 6/2, Bologna, Italy
[i] Italian Space Agency, Via del Politecnico, I-00133 Roma, Italy
[l] University of Napoli "Federico II", Via Cintia, I-80126 Napoli, Italy
[m] INFN-Sezione di Firenze, Via Sansone 1, I-50019 Sesto Fiorentino (Firenze), Italy
[n] University of Roma "Tor Vergata", Via della Ricerca Scientifica 1, I-00133 Roma, Italy
[o] INFN-LNF, Via E. Fermi 54, I-00044 Frascati (Roma), Italy

PoS(ICRC2023)689